

# Real-Time Debris Patterns for Ballistic Missile Launches

Jon D. Collins,\* Moroni Jameson Jr.,†  
*J.H. Wiggins Company, Redondo Beach, Calif.*

and

J.L. Jantz‡  
*Space and Missile Test Center, Vandenberg Air Force Base, Calif.*

A methodology was developed to predict in real time the probabilistic boundaries of the dispersion of debris from a missile destroyed at that instant of time in flight. The method uses prelaunch tabulated data based on statistical characterization of wind, missile trajectory, and missile breakup characteristics, which are input into a real-time program and transformed from the predicted to actual conditions to compute the debris pattern. The method was evaluated for accuracy and efficiency for a variety of flight conditions, missile types, and display presentation. In addition, a comparison with the actual debris impacts from an aborted launch showed that the debris landed within the predicted debris pattern.

## Background

FOR many years missile flight safety at the major missile ranges has depended upon various plotboard displays of missile present position and its instantaneous vacuum impact point, in conjunction with abort lines and other control plots to provide missile performance (go/abort) information to the missile flight safety officer. The advent of improved computers and the real-time use of cathode ray tubes has opened up new opportunities for displaying useful information to assist the go/abort decision. One new opportunity has been the creation of the debris pattern display, which presented an envelope of the possible impact points of debris, if the missile were to be destroyed at that instant in time. The real-time debris pattern display must contain the following items: 1) a best estimate of the locus of debris impact points resulting from a decision to abort the missile in flight, 2) a statistical envelope within which the debris will be contained with a specified probability, 3) an indication of the potential shift of the debris impact points occurring between the time a decision to abort the mission has been made and the time that the successful abort will occur, and 4) mission constraints in the form of overflown population centers and impact limit lines.

The debris pattern envelope, as developed, is composed of two distinct envelopes. The first is a region within which debris will land in the event of vehicle breakup, and the second is a region within which a nonthrusting but intact vehicle will impact (see Fig. 1).

For this display to provide a significant improvement in decision making over the existing plotboards, it must give an accurate and timely picture of the region hazarded. Accuracy of representation is significant, since an erroneous representation of pattern size or orientation either can give the missile flight safety officer a false sense of security or, alternatively, erroneously alert him to nonexistent hazardous conditions. Timely representation means that the algorithm employed must be rapid enough to update the pattern each time the pat-

tern has changed enough to create a perceptible difference in the display. The requirement for a smooth transition results in a display regeneration frequency of 5-10 times/sec.

Implementation of this kind of display required adopting a strategy of precomputing as many of the parameters characterizing the debris pattern as possible prior to launch, adopting certain, carefully chosen, simplifying assumptions, and reserving for real-time computation only those quantities which could not be precomputed. This paper will detail the development of the mathematical models employed in the generation of the debris pattern display.

## Overview of the Concept

The problem divides into two major computational difficulties: 1) the need for rapid computation of a number of drag-corrected impact points in real time, and 2) the need for rapid computation of the statistical dispersions of these impact points. Both computations are very difficult to do rapidly, the first because of the many integration steps required, and the second because it involves perturbations of the integrated drag-corrected trajectories. The initial objective of the work, therefore, was to find similarities, transformations, etc., that would allow bypassing or simplifying many of the computations during real-time operation.

Before proceeding with the methodology, it is worthwhile to examine the basic physical principles involved in the dispersion of debris. Figure 2 shows the paths of the falling debris

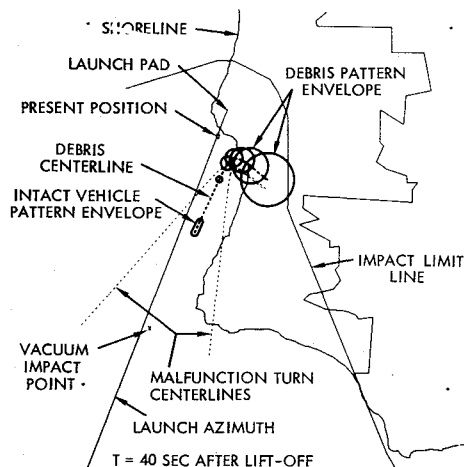


Fig. 1 Basic elements of the debris pattern display.

Received May 17, 1975; revision received Feb. 4, 1976. This work was sponsored by the U.S. Air Force Space and Missile Test Center (SAMTEC) under Contract No. F04701-72-C-0147. The methods and computer programs described in this paper resulted from the collective effort of a number of people. The authors wish to acknowledge the technical contributions of James B. Baeker, Buchanan Cargal, R.T. Gabler, Jerold M. Haber, and Bruce Kennedy.

Index categories: Safety; LV/M Flight Testing; Computer Technology and Computer Simulation Techniques.

\*Vice President, Associate Fellow AIAA.

†Manager, Vandenberg Air Force Base Field Office.

‡Aerospace Engineer.

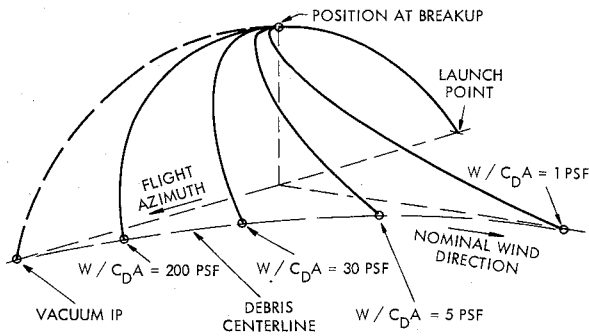


Fig. 2 Influence of Ballistic Coefficient ( $W/C_D A$ ) and wind upon fragment trajectories.

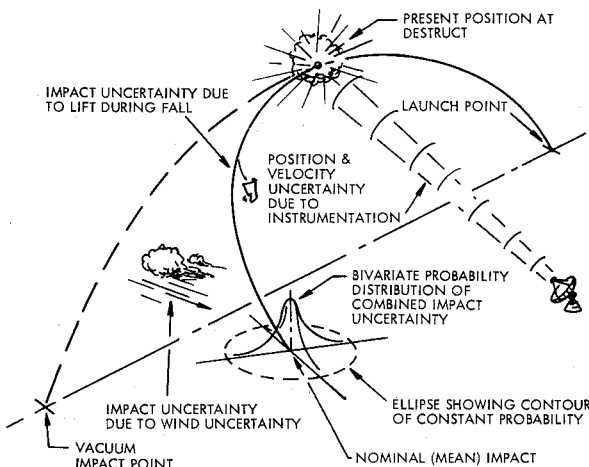


Fig. 3 Fragment impact uncertainty.

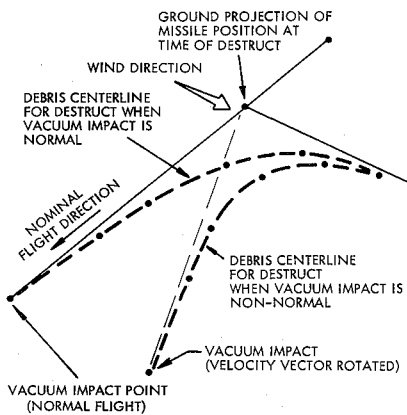


Fig. 4 Comparison of normal and nonnormal centerlines.

resulting from missile breakup at a particular point in time. If a missile fragment has no drag (i.e., the fragment moves in a vacuum), the impact point will be in the direction of the flight azimuth. This point is noted as the vacuum IP in Fig. 2. At the other extreme is the fragment having a low weight-to-drag ratio (low ballistic coefficient, i.e., low  $W/C_D A$ ). At the instant of release, these low  $W/C_D A$  fragments decelerate very rapidly and approach terminal velocity in a matter of seconds. At that point, the dominant dispersive force is wind, and the fragment falls at terminal velocity while drifting at the wind speed. This is shown in Fig. 2 by the ballistic path of the fragment having  $W/C_D A = 1$  psf. (1 psf can be typical of missile skin pieces and panels.) Fragments with higher ballistic coefficients are not as influenced by the wind and, depending upon their drag characteristics, fall along a locus which is called the debris centerline.

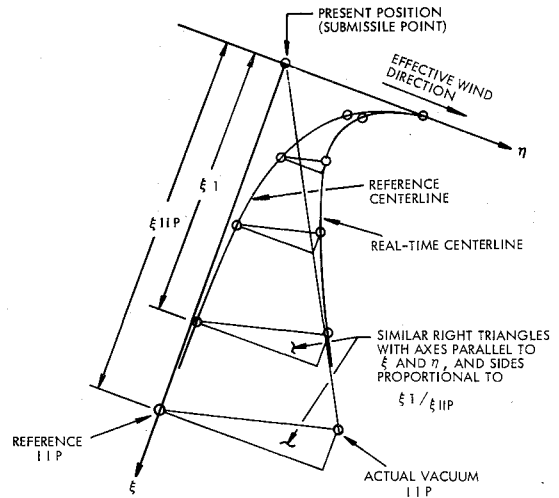


Fig. 5 Centerline transformation.

The debris centerline, noted in Fig. 2, reflects the predicted average impact points of the debris. There are many variables which can disturb these expected impact points; among them are variability of the wind with respect to time, accurate prediction (measurement) of the wind, drag and lift of a missile fragment, atmospheric density, instrumentation and filtering error in establishing actual missile position and velocity at the time of destruct, and perturbation velocities to the missile fragment as a result of explosive forces at the time of destruct.

Figure 3 depicts these uncertainties acting upon the flight of a typical fragment. The sources of impact uncertainty are statistically independent and relatively small compared to the flight path. Consequently, the assumption was made that the combined impact density function was bivariate normal. The contours of constant probability are, therefore, ellipses as shown in Fig. 3.

### Computation of Drag-Corrected Impact Points in Real Time

The information in Fig. 2 suggests two major points: 1) impact points of very light debris are not influenced by rapid or instantaneous changes in the missile velocity vector but are influenced primarily by the wind; and 2) impact points of very heavy debris are not influenced by the wind but change according to the movement of the vacuum impact point. Thus two debris centerlines based on the missile being initially at the same position, but with one having a rotated velocity vector, will appear, as shown in Fig. 4.

It is evident that, if a mathematical transformation is available to move from the normal (predicted) to the non-normal (real time) centerline without having to recompute the drag-corrected impact points, then the computation of a nominal centerline based upon drag-corrected impact points may be made prior to the launch time and transformed to the actual centerline in real-time operation. The method that was selected is shown in Fig. 5. Prior to launch, a series of drag-corrected impact points (centerlines) is computed for failures at successive missile altitudes based on expected trajectory characteristics. These centerlines, referenced to the altitude of the missile at the time of breakup, are computed with the expected (measured) wind rotated to be  $90^\circ$  from the direction of flight. This results in separating, to some extent, the drag effect on the debris (in the downrange direction) from the wind effect (in the crossrange direction). In real-time operations, the actual vacuum impact point is computed in this coordinate system, and all intermediate drag-corrected impact points are computed by means of translating the reference values from the prelaunch computer run via a set of similar triangles. These reference values are obtained by

taking the actual missile altitude and interpolating a corresponding reference centerline from the stored centerlines. This centerline transformation has been tested extensively and works very effectively as long as the actual missile altitude and velocity are within 20% of that expected.

### Computation of Impact Uncertainties in Real Time

If the missile altitude is not excessively above or below that which was expected, the impact uncertainties are relatively independent of the lateral motion of the falling missile. Therefore, the most economical approach is to develop a set of impact uncertainty parameters for the nominal missile performance and to use these data for the missile in real time. This results in shifting the heavy computational load to a time prior to the launch, thus permitting the use of tabular data in real time.

### Computation of Impact Uncertainties from Individual Error Sources

Seven sources of impact uncertainty exist, of which two (atmospheric density and drag) were omitted. The density uncertainty can be omitted by updating the density information used by the mathematical models just prior to the prelaunch computations for a missile flight. The drag uncertainty was omitted, because it is oriented along the centerline and does not contribute to the more significant crossrange effect. If it is intended that the dispersion encompasses a particular fragment impact in the directions both along and perpendicular to the centerline, however, the drag uncertainty must be included.

The procedure used in evaluating the five dispersion contributions is basically the same. A linear relationship is developed between the perturbation of the coordinate of the source of the uncertainty and the perturbation of the impact coordinates:

$$\begin{Bmatrix} dx \\ dy \end{Bmatrix} = \begin{bmatrix} \partial x/\partial p_1 & \partial x/\partial p_2 & \cdots \\ \partial y/\partial p_1 & \partial y/\partial p_2 & \cdots \end{bmatrix} \begin{Bmatrix} dp_1 \\ dp_2 \\ \vdots \end{Bmatrix} = \left[ \frac{\partial(x,y)}{\partial(p_1, p_2, \dots)} \right] \begin{Bmatrix} dp_1 \\ dp_2 \\ \vdots \end{Bmatrix} \quad (1)$$

where  $x$  and  $y$  are an orthogonal set of coordinates with origin at the nominal impact point, and  $p_1, p_2$ , etc., are measures of the coordinates of the error source (e.g., errors in  $R, A, E, \dot{R}$  measurements of missile position by the tracking radar). The matrix is the linear transformation between the two coordinate systems.

If the error source can be described in the form of a covariance matrix,

$$[\Sigma_p] = \begin{bmatrix} \sigma_{p_1}^2 & \sigma_{p_1 p_2} & \cdots \\ \sigma_{p_2 p_1} & \sigma_{p_2}^2 & \cdots \\ \cdots & \cdots & \cdots \end{bmatrix} \quad (2)$$

then the covariance for the impact dispersion becomes

$$[\Sigma_I] = \begin{bmatrix} \sigma_x^2 & \sigma_{xy} \\ \sigma_{yx} & \sigma_y^2 \end{bmatrix} = \left[ \frac{\partial(x,y)}{\partial(p_1, p_2, \dots)} \right] [\Sigma_p] \times \left[ \frac{\partial(x,y)}{\partial(p_1, p_2, \dots)} \right]^T \quad (3)$$

where  $\sigma_x^2$  is the variance of the random variable  $x$ ,  $\sigma_y^2$  is the variance of the random variables  $y$ , and  $\sigma_{xy}$  is the covariance of  $x$  and  $y$ .

Table 1 contains the basic descriptions of the dispersion error sources and the transformation matrices. The wind variability uncertainty is the uncertainty due to the changing with time. Wind measurements at a series of altitudes and times were made, reduced, and summarized statistically in Ref. 1, which gives the uncertainties for a 6-hr period. If the launch is  $t$  hr after the measurement, the uncertainties are scaled by the equation  $a(1 - e^{-bt})$  where  $a$  and  $b$  are factors which normalize to one at 6 hr and account for increasing uncertainty with a time delay.<sup>2</sup> A second uncertainty, the wind covariance matrix due to wind measurement, is based on the capabilities of the wind measurement equipment. The transformation matrix for the winds is based upon the debris falling at terminal velocity and moving laterally with the wind.

The uncertainty caused by tracking error first is expressed by the covariance matrix  $[\Sigma_{TR}]$ . The transformation matrix is based upon a perturbation of the Keplerian vacuum equations, with the values scaled down according to the drag effect upon the trajectory range. The impact uncertainty because of explosion uses the same basic transformation (except for coordinate adjustment), with a velocity covariance matrix composed of three diagonal elements, which usually are treated as equal.

The treatment of impact uncertainty due to lift is heuristic and deserves further analysis using six-degree-of-freedom analysis which, along with the difficulty of obtaining aerodynamic parameters, is very expensive. The data shown in the table are based on conclusions inferred from a modified six-dimensional study performed for Apollo.<sup>3</sup>

After each of the impact covariances have been computed, they can be added, because of statistical independence, to form the composite covariance matrix:

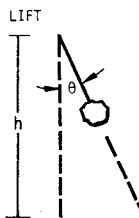
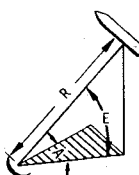
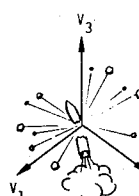
$$[\Sigma_I]_{\text{total}} = [\Sigma_I]_{wv} + [\Sigma_I]_{wm} + [\Sigma_I]_v + [\Sigma_I]_L \quad (4)$$

### Basic Display Design and Generation

The elements of the debris pattern display are shown in Fig. 1. The debris dispersions are presented as circles with radii equal to the major axes of the ellipses. This display of circles is simplest and fastest on the computer but does produce dispersions slightly larger in one dimension than the true elliptical dispersions. A third method of dispersion display, involving an envelope containing all of the circles or ellipses, was developed, but the logic, which had to handle a number of unusual nested and partially nested situations, required computer times greater than 75 msec which, with other required real-time operation functions, exceeded the time budget.

There are two additional items shown in the display: intact vehicle pattern envelope and malfunction turn centerlines. The intact vehicle pattern envelope surrounds the dispersion for an intact missile (not broken up into debris) coming in broadside and an intact missile coming in at zero angle of attack. This information is provided in case the safety officer has the option to shut off the fuel rather than destroy the vehicle. The malfunction turn centerline is developed using the centerline transformation technique and represents a centerline  $T$  seconds ahead, if the missile were to go into a hard right or left turn at this instant.

Table 1 Impact dispersion error sources.

ERROR SOURCE	STATISTICAL FORMULATION OF ERROR SOURCE	TRANSFORMATION MATRIX	IMPACT UNCERTAINTY FORMULATION
WIND VARIABILITY	COVARIANCE MATRIX OF 6 HR WIND UNCERTAINTIES AT MANY ALTITUDES $[\epsilon_{WV}] = \begin{bmatrix} \sigma_{E_1}^2 & \sigma_{E_1 N_1} & \cdot & \cdot \\ \sigma_{E_1 N_1} & \sigma_{N_1}^2 & \cdot & \cdot \\ \cdot & \cdot & \sigma_{E_2}^2 & \cdot \\ \cdot & \cdot & \cdot & \cdot \end{bmatrix}$ WHERE $E_i$ IS THE WIND VELOCITY IN THE EASTERLY DIRECTION AT ALTITUDE $i$ , ETC.	$[T_W] = \begin{bmatrix} \frac{\partial X}{\partial E_1} & \frac{\partial X}{\partial N_1} & \frac{\partial X}{\partial E_2} \\ \frac{\partial Y}{\partial E_1} & \frac{\partial Y}{\partial N_1} & \frac{\partial Y}{\partial E_2} \end{bmatrix}$ $= \begin{bmatrix} \frac{\partial(X,Y)}{\partial(E_1, N_1, E_2, N_2, \dots)} \end{bmatrix}$ WHERE $X, Y$ ARE DISPLACEMENTS OF THE IMPACT POINT IN A SELECTED SET OF ORTHOGONAL DIRECTIONS	$[\epsilon_I]_{WV} = \frac{t}{6} [T_W] [\epsilon_{WV}] [T_W]^T$ <p><math>t</math> IS THE TIME FROM WIND MEASUREMENT TO LAUNCH. UNCERTAINTY SCALES AS <math>\left(\frac{t}{6}\right)^{1/2}</math></p>
WIND MEASUREMENT UNCERTAINTY	$[\epsilon_{WM}] = \begin{bmatrix} \sigma_{E_1}^2 \\ \cdot \\ \cdot \\ \cdot \end{bmatrix}$ ETC.  CAN INPUT SPECIFIC SCALED UNCERTAINTIES FOR GMD-1, GMD-4, AND JIMSPHERE	$[T_W]$ , SAME TRANSFORMATION AS ABOVE	$[\epsilon_I]_{WM} = [T_W] [\epsilon_{WM}] [T_W]^T$
LIFT  DRIFT DUE TO LIFT (NO WIND)	REPLACE THE INTEGRATED EFFECT OF A STOCHASTIC RANDOM LIFT ORIENTATION WITH AN EFFECTIVE $L/D$ UNCERTAINTY, $\sigma_{L/D}$ . $\sigma_{L/D} = \begin{cases} .01, \text{ BLUNT OBJECTS} \\ .03, \text{ INTERMEDIATE SHAPES} \\ .05, \text{ FLAT PANEL-LIKE OBJECTS} \end{cases}$	$x(\text{OR } y) = \left(h L/D\right)$ <p><math>h</math>, THE ALTITUDE HAS AN ALLOWABLE MAXIMUM OF 60,000 FT.</p>	$[\epsilon_I]_L = \left(h \sigma_{L/D}\right)^2 \begin{bmatrix} 1 & 0 \\ 0 & 1 \end{bmatrix}$
TRACKING ERROR 	COVARIANCE MATRIX OF TRACKING ERRORS $[\epsilon_{TR}] = \begin{bmatrix} \sigma_R^2 & 0 & 0 & \sigma_{RR} \\ 0 & \sigma_A^2 & 0 & 0 \\ 0 & 0 & \sigma_E^2 & 0 \\ \sigma_{RR} & 0 & 0 & \sigma_R^2 \end{bmatrix}$	$[T_{TR}] = \begin{bmatrix} \frac{\partial X}{\partial R} & \frac{\partial X}{\partial A} & \frac{\partial X}{\partial E} & \cdot \\ \frac{\partial Y}{\partial R} & \frac{\partial Y}{\partial A} & \frac{\partial Y}{\partial E} & \cdot \end{bmatrix}$ $= \begin{bmatrix} \frac{\partial(X,Y)}{\partial(R,A,E,R,A,E)} \end{bmatrix}$ <p>THE PARTIAL DERIVATIVES ARE TAKEN WITH RESPECT TO THE KEPLERIAN "NO ATMOSPHERE" BALLISTIC RELATIONS AND CORRECTED FOR DRAG.</p>	$[\epsilon_I]_{TR} = [T_{TR}] [\epsilon_{TR}] [T_{TR}]^T$
EXPLOSION VELOCITY 	COVARIANCE MATRIX OF VELOCITY IMPULSE $[\epsilon_V] = \begin{bmatrix} \sigma_{V_1}^2 & 0 & 0 \\ 0 & \sigma_{V_2}^2 & 0 \\ 0 & 0 & \sigma_{V_3}^2 \end{bmatrix}$	$[T_V] = \begin{bmatrix} \frac{\partial X}{\partial V_1} & \frac{\partial X}{\partial V_2} & \frac{\partial X}{\partial V_3} \\ \frac{\partial Y}{\partial V_1} & \frac{\partial Y}{\partial V_2} & \frac{\partial Y}{\partial V_3} \end{bmatrix}$ $= \begin{bmatrix} \frac{\partial(X,Y)}{\partial(V_1, V_2, V_3)} \end{bmatrix}$ <p>THE PARTIAL DERIVATIVES ARE TAKEN WITH RESPECT TO THE KEPLERIAN "NO ATMOSPHERE" BALLISTIC RELATIONS AND CORRECTED FOR DRAG.</p>	$[\epsilon_I]_V = [T_V] [\epsilon_V] [T_V]^T$

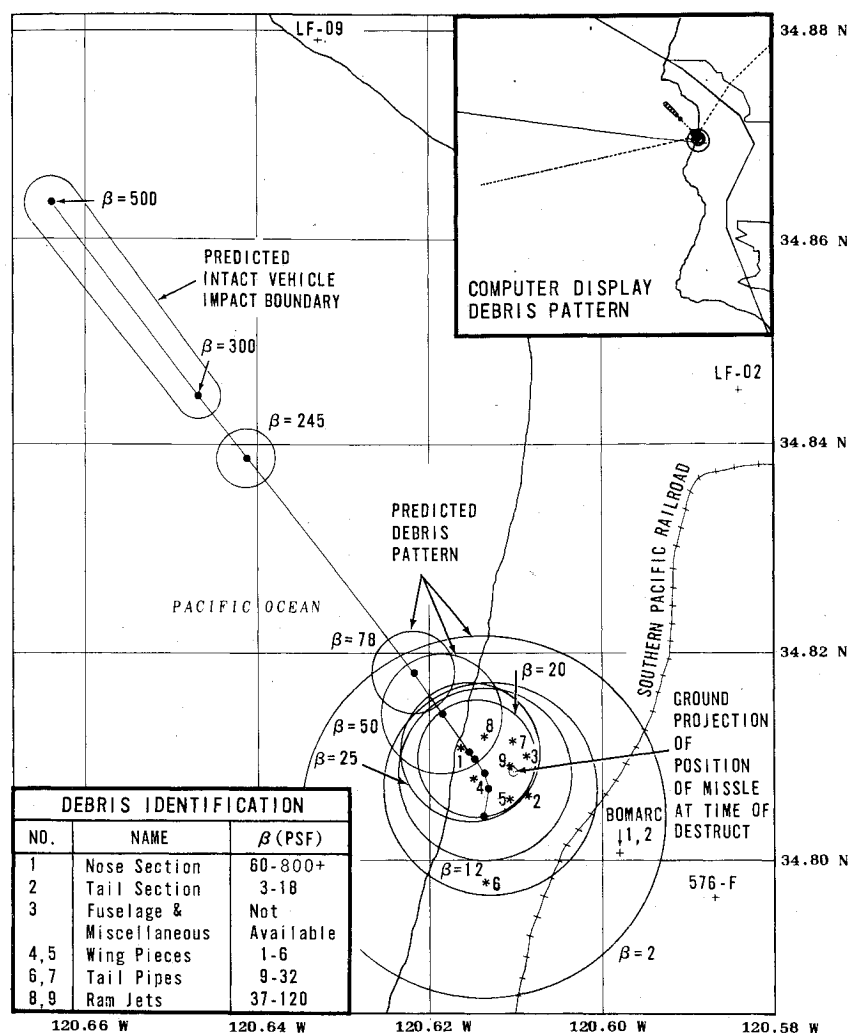


Fig. 6 Predicted debris pattern and actual impact points of BOMARC debris.

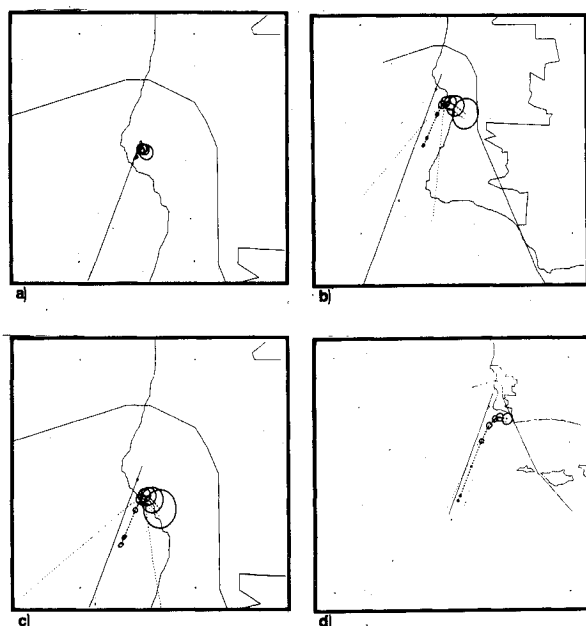


Fig. 7 Debris pattern sequence (Thor-Delta): a)  $T + 20.0$ ; b)  $T + 40.0$ ; c)  $T + 31.0$ ; d)  $T + 80.0$ .

### Debris Pattern Tests and Examples

On Sept. 11, 1973, a BOMARC failed and was destroyed after 21 sec of flight. After the flight, debris were located and

identified. Ranges of the ballistic coefficients of the debris were computed. Narrower ranges could not be specified, because there were no specific photographic data of the debris and no evidence whether the debris tumbled or stabilized during the fall. Figure 6 shows a detail of the debris pattern at the instant of destruct. Plotted on the debris pattern are the impact point of the debris. The patterns are approximately  $2\sigma$  patterns which represent boundaries having at least an 86% probability of containing the debris impact points. It is evident that the statistical predictions adequately contain the debris impacts. It also points out the fact that rarely can debris be described by a specific ballistic coefficient, but more adequately by a range of values. Most debris, however, tend to land toward the low ballistic coefficient end of the pattern, which indicates a tumbling rather than a stable head-in fall, as one might expect.

### Debris Pattern Sequence

A sequence of patterns (in this case, ellipses) is shown in Fig. 7 for the simulated launch of a Thor-Delta. Note the growth of the individual dispersions and then the gradual stretching out of the pattern as the fragments having the higher ballistic coefficients move downrange more rapidly. Sequences were also computed at approximately 0.2 sec intervals and made into motion pictures simulating the real-time launch environment.

### Conclusion

A method for computing the predicted dispersion of fragments has been formulated and demonstrated. The

statistical portion of the model incorporates the propagation of errors in position, velocity, wind, lift, etc., by means of linear propagation of covariance. The mean drag-corrected impact points are computed by adjusting the vacuum impact points, using predetermined adjustments for drag and wind effects. The method is structured for rapid numerical computation (real time) and has been demonstrated to maintain acceptable accuracy.

### References

- <sup>1</sup>Stern, R.G., "Six-Hour Wind Variability at Pt. Arguello," Aerospace Corp., El Segundo, Calif., Rept. TOR-1001(23)5-1, July 1966.
- <sup>2</sup>Valley, S.L., (ed.), *Handbook of Geophysics and Space Environments*, McGraw-Hill, New York, 1965.
- <sup>3</sup>Marx, M., "Apollo Forced Entry Debris Dispersion Study," TRW Systems, Redondo Beach, Calif., Note 68-FMT-648, April 1968.

*From the AIAA Progress in Astronautics and Aeronautics Series . . .*

## **SPACE POWER SYSTEMS ENGINEERING—v. 16**

*Edited by George C. Szego, Institute for Defense Analyses, and J. Edward Taylor, TRW Inc.*

The sixty-two papers in this volume concern electric power systems for space vehicles, covering requirements and applications, nuclear system development, chemical system development, and MHD power systems.

Papers treat radioisotope power systems, the SNAP series of reactors, nuclear propulsion systems, electric propulsion systems, a comparison and combination of both for space missions, and an optimized nuclear-electric system.

Solar cell power systems are optimized and compared with solar-thermionic systems and Brayton-cycle solar dynamic systems, all of which are posited for specific space missions. Fuel cells systems are analyzed and compared. Rankine cycle generators are proposed for specific applications.

Solar concentrators for power generation are proposed and evaluated, with applications to both Rankine and Brayton cycle conversion systems. Thermionic converters are examined and modeled.

Other papers examine fuel cell chemistry and engineering. Various cells, using various power sources, are considered. Batteries of various types are considered for use with fuel cell systems, and various control systems are proposed.

*1302 pp., 6 x 9, illus, \$29.50 Mem. & List*

TO ORDER WRITE: Publications Dept., AIAA, 1290 Avenue of the Americas, New York, N. Y. 10019